Cerebral Cortex September 2015;25:2658–2669
doi:10.1093/cercor/bhu064
Advance Access publication April 11, 2014

The Richness of Task-Evoked Hemodynamic Responses Defines a Pseudohierarchy of Functionally Meaningful Brain Networks

Pierre Orban[1,2], Julien Doyon[1,3], Michael Petrides[6], Maarten Mennes[7,8], Richard Hoge[1,4] and Pierre Bellec[1,5]

[1]Functional Neuroimaging Unit, Centre de Recherche de l'Institut Universitaire de Gériatrie de Montréal, [2]Department of Psychiatry, [3]Department of Psychology, [4]Department of Physiology and Biomedical Engineering, [5]Department of Computer Science and Operations Research, University of Montreal, Montreal, Quebec, Canada, [6]Cognitive Neuroscience Unit, Montreal Neurological Institute, McGill University, Montreal, Quebec, Canada, [7]Department of Cognitive Neuroscience, Radbout University Nijmegen Medical Center, Nijmegen, The Netherlands and [8]Donders Institute for Brain, Cognition and Behavior, Radbout University Nijmegen, Nijmegen, The Netherlands

Address correspondence to Pierre Orban, CRIUGM, 4545 Queen Mary, Montreal, QC, Canada H3W 1W5. Email: pierre.orban@criugm.qc.ca.

Functional magnetic resonance imaging can measure distributed and subtle variations in brain responses associated with task performance. However, it is unclear whether the rich variety of responses observed across the brain is functionally meaningful and consistent across individuals. Here, we used a multivariate clustering approach that grouped brain regions into clusters based on the similarity of their task-evoked temporal responses at the individual level, and then established the spatial consistency of these individual clusters at the group level. We observed a stable pseudohierarchy of task-evoked networks in the context of a delayed sequential motor task, where the fractionation of networks was driven by a gradient of involvement in motor sequence preparation versus execution. In line with theories about higher-level cognitive functioning, this gradient evolved in a rostro-caudal manner in the frontal lobe. In addition, parcellations in the cerebellum and basal ganglia matched with known anatomical territories and fiber pathways with the cerebral cortex. These findings demonstrate that subtle variations in brain responses associated with task performance are systematic enough across subjects to define a pseudohierarchy of task-evoked networks. Such networks capture meaningful functional features of brain organization as shaped by a given cognitive context.

Keywords: clustering analysis, fMRI, functional connectivity, motor preparation and execution, multiscale task-evoked networks

Introduction

In the past two decades, task-based functional magnetic resonance imaging (fMRI) has been used to uncover brain substrates of a myriad of cognitive processes. However, in the vast majority of fMRI studies, activation maps provide a sparse representation of brain function: Only a handful of brain areas are reported as significantly engaged in a task. Yet, it is unlikely that only brain areas withheld by an arbitrary statistical threshold are involved in stimulus processing. Indeed, a large number of brain areas might falsely be described as nonactive. This is in part due to the differential contrasts commonly used in analysis models, and can also be attributed to limited statistical power resulting from a limited number of task trials and/or participants and the use of rigid predictive response models. Accordingly, Worsley (2004), a pioneer of fMRI statistics, stated that, "in reality, every voxel must be affected by the stimulus, perhaps by a very tiny amount; it is impossible to believe that there is never any signal at all."

Worsley's statement was recently tested by Gonzalez-Castillo et al. (2012), who collected nearly 10 h of fMRI data in 3 participants engaged in a visual task. A model-free analysis of this massive amount of data demonstrated significant task-evoked responses across the entire brain, and thus not limited to visual cortex. In addition, brain regions exhibited an overwhelming variety in the shape of their task-evoked response. A critical implication is that determining whether a brain region is active or inactive is an ill-posed problem and a paradigm shift in studying cognition with task-based fMRI is warranted. Instead of indexing brain activity in an "on versus off" fashion, the challenge becomes to systematically describe the organization of this rich variety of task-evoked dynamics across the brain. In their approach, Gonzalez-Castillo et al. (2012) demonstrated the possibility of grouping brain regions with similar dynamics into task-evoked networks at the single-subject level. Networks were derived at multiple scales, ranging from 2 to 70 networks, in line with the notion that the brain is hierarchically organized (Smith et al. 2009; Meunier et al. 2010; Power et al. 2011; Yeo et al. 2011; Kelly et al. 2012).

At present, it is unclear to which extent those task-evoked hierarchies capture meaningful organizational features of the brain in action. It is also unknown whether the spatial distribution of such hierarchical networks and their associated temporal dynamics are consistent across subjects. In this work, we sought to determine whether stable multiscale task-evoked networks could be inferred at the group level. We investigated a motor control task that has been extensively documented in monkey and human research. This allowed to evaluate the biological plausibility of the derived task-evoked networks.

To study the variety of brain dynamics, we relied on the well-established finite impulse response (FIR) estimation (Dale and Buckner 1997). This model-free analysis derives a non-parametric estimate of the task-evoked response by averaging multiple events. In practice, however, the FIR technique is usually applied to only a few a priori brain regions, because task-evoked dynamics are too rich to be reviewed and interpreted at every possible location in the brain. Multivariate techniques such as independent component analysis, principal component analysis, or clustering approaches can be used to reduce the spatial dimensionality of task-evoked brain activity (Calhoun et al. 2001; Svensén et al. 2002; d'Avossa et al. 2003; Smolders et al. 2007; Metzak et al. 2011). However, these studies only reported coarse levels of decomposition at the group level, that is, describing around 5 task-evoked networks. Here, we used a recently developed method, called bootstrap analysis of stable clusters (BASC), that has the potential to identify stable, group-level task-evoked networks at multiple

scales, up to tens or even hundreds of networks (Bellec et al. 2010). Applied to FIR estimates, BASC uses hierarchical clustering at the individual level, to identify networks of regions exhibiting similar FIR shapes. Then, at the group level, BASC delineates networks that are spatially consistent across subjects.

We applied BASC to event-related fMRI data of 17 participants who performed a delayed sequential motor task. Task trials were composed of a preparation period followed by self-initiated execution of a sequence of finger movements. We pursued 2 main objectives with our analyses. First, we conducted exploratory analyses aimed at evaluating the spatial stability of task-evoked networks and examined whether meaningful differences in temporal dynamics could be observed at the group level. We examined task-evoked networks using different clustering scales, ranging from two to several hundreds of networks, that were determined using an automated, data-driven strategy (Bellec 2013). Secondly, we conducted hypothesis-driven analyses to assess the biological relevance of the observed task-evoked networks. In particular, previous studies using electrophysiology in monkeys have illustrated that, in the frontal lobe, the presupplementary motor area (pSMA), the SMA proper, the lateral premotor cortex (Pmd), and the primary motor cortex (PMC) all contain neurons that fire in response to both motor preparation and execution (Okano and Tanji 1987; Romo and Schultz 1987; Mushiake et al. 1991). However, they do so in different proportions following a rostro-caudal functional gradient, from regions involved in the high-level cognitive processes supporting preparation to those tightly coupled with motor execution (Passingham et al. 2002; Nachev et al. 2008; Badre and D'Esposito 2009). In accordance with these observations, we predicted that numerous task-evoked networks would emerge driven by their relative implication in the preparation versus execution phases, not only in the frontal lobe but also throughout the cortex. Finally, in accordance with the organization of long-range anatomical pathways (Alexander and Crutcher 1990; Middleton and Strick 2000; Bostan et al. 2013), we hypothesized that the gradient observed at the cortical level would propagate to subcortical structures such as the cerebellum and basal ganglia.

Materials and Methods

All scripts used to conduct the analysis reported in this paper can be found on github: http://github.com/pbellec/basc_fir_paper, last accessed on 24 March 2014. See the README.md file for licensing and a description of content.

Experimental Set-up

Population

A total of $N = 17$ volunteers (12 men and 5 women), aged between 21 and 28 years, gave informed consent to participate in this study, which was approved by the local ethics committee at the Research Center of the Geriatric Institute, University of Montreal, Canada. All subjects were right-handed and without a history of neurological or psychiatric disorder.

Experimental Task

A delayed sequential finger-tapping task was administered in a single run, with 60 trials interspersed with rest epochs lasting 13 s on average (jittering ranging from 8 to 18 s). We used a motor control task that requires the execution of internally triggered rather than externally triggered movements, because the former is associated with enhanced activity in the frontal lobe (Boecker et al. 2008). Each trial was composed of 2 components: A preparation period followed by the execution of an 8-element finger-tapping sequence (1 2 3 4 1 2 3 4; where 1, 2, 3, and 4, respectively, refer to the index, middle, ring, and little fingers). Movements were performed with the left, nondominant hand. After each rest epoch, during which a black screen was displayed, the brief appearance (500 ms) of a yellow square indicated that subjects had to mentally plan to self-initiate the sequential movements, without further external cueing (mean preparation duration = 7.4 ± 0.7 s). As soon as the first finger movement was initiated, a blue square displayed for 500 ms at the center of the black screen, confirmed the beginning of the execution phase (mean execution duration = 3.7 ± 0.2 s). Subjects were instructed to start tapping after a period of a few seconds (~7 s) and to produce finger taps at a comfortable pace without external constraint (~2 Hz). A prescanning training session was conducted to reduce variability in duration for each task component, and to ensure that a minimal duration of a few seconds was reached for proper analysis of fMRI data. Trials with preparation or execution durations beyond 1.96 standard deviations of the individual means, and those that contained an erroneous finger tap, were excluded from further analysis. An average of 47.4 (±5.7) trials per subject were included as events of interest in all fMRI data analyses.

Imaging

Brain imaging data were acquired on a 3-T MRI scanner (Magnetom Tim Trio, Siemens) with a 12-channel head coil. An average total of 702 functional volumes (range 658–753) were recorded per subject while they performed the motor task. T_2*-weighted images were obtained using a blood oxygen level-dependent sensitive, single-shot echo planar sequence (repetition time = 2000 ms; echo time = 30 ms; flip angle = 90°; matrix size = 64 × 64; voxel size = 3 × 3 × 4 mm^3; gap = 15%; 33 slices). Structural T_1*-weighted scans were acquired using a turbo flash sequence with an inversion pulse (repetition time = 2300 ms; echo time = 3 ms; flip angle = 9°; matrix size = 256 × 256; voxel size = 1 × 1 × 1 mm^3; 176 slices).

Preprocessing of Imaging Data

Realignment and Artifact Reduction

The fMRI data were preprocessed using the fMRI preprocessing pipeline implemented in the neuroimaging analysis kit, NIAK version 0.6.4.3 (http://www.nitrc.org/plugins/mwiki/index.php/niak:FmriPreprocessing064, last accessed on 24 March 2014) (Bellec et al. 2012). Each dataset was corrected of interslice difference in acquisition time, rigid body motion, and slow time drifts (high-pass filter with a 0.01 Hz cutoff). For each subject, the mean motion-corrected volume of all the datasets was coregistered with a T_1 individual scan using Minctracc (Collins et al. 1994), which was itself nonlinearly transformed to the Montreal Neurological Institute (MNI) nonlinear template using the CIVET pipeline (Zijdenbos et al. 2002). The functional volumes were resampled to MNI space at a 3-mm isotropic resolution and spatially smoothed with a 6-mm isotropic Gaussian kernel.

Region Growing

For each voxel and each event, the fMRI time samples following the onset of the event were interpolated on a fixed temporal grid (length: 20 s and step: 1 s). The FIR estimate at each voxel was the average of all aligned events, normalized to an unit energy (sum of squares of all time points) (Supplementary Fig. 1). This normalization was applied to ensure that the subsequent clustering would be driven by the shape of the FIR rather than the absolute amplitude of the response. To reduce the computational burden of the analysis, we analyzed FIR responses for 957 regions covering the gray matter. These regions were derived using a region-growing algorithm (Bellec et al. 2006) applied on voxel-wise FIR estimates, with regions of a controlled size (threshold: 1000 mm^3). All subsequent cluster analysis was performed on *de novo* FIR estimates derived from average regional fMRI time series.

Bootstrap Analysis of Stable Clusters

Consensus Clustering

Next, we applied a cluster analysis on the regional FIR estimates to identify networks that consistently exhibited similar FIR shapes in individual subjects, and were spatially stable across subjects. This analysis was carried using the BASC framework (Bellec et al. 2010) aimed at quantifying the reproducibility of a cluster analysis, while providing a cluster solution that captures the most stable features across many replications. BASC proceeds by repeating a clustering operation (here, a hierarchical agglomerative clustering with Ward's criterion) 1000 times, and computes the frequency with which each pair of regions was assigned to the same cluster, called pairwise stability. The set of all pairwise stability measures forms a region × region matrix, which is in turn fed into a clustering procedure to derive consensus clusters. The consensus clusters are composed of regions with a high average probability of being assigned to a certain cluster across all replications, hence the name consensus.

Multilevel (Individual and Group) Cluster Analysis

We first applied the consensus clustering technique at an individual level, to quantify the stability of the FIR-driven clusters. In this case, the clustering applied to the similarity of average FIR across regions and the average FIR estimates were replicated through the bootstrap of individual trials. Subsequently, consensus clustering was applied to the average of all individual stability matrices to identify group clusters, with stable association across subjects. The stability of these group clusters was itself assessed by replicating the group cluster via bootstrapping of subjects in the group. Finally, we generated a final consensus clustering based on the group stability matrix. Schematics of the BASC analysis and more details on the algorithm can be found in Supplementary Figures 2 and 3.

Scale Selection

It is important to note that, at each level, the consenus clustering was carried out with a specific number of clusters (scales). Accordingly, 3 parameters needed to be selected in our multilevel clustering procedure: *K*, *L*, and *M*, which correspond to the individual, group, and final numbers of clusters, respectively. Using a "multiscale stepwise selection" method, we determined a subset of scales that provided an accurate summary of the stable clusters across all scales (Bellec 2013). The selected values for *K/L/M* were *2/2/2*, *5/4/4*, *10/10/9*, *30/27/34*, *120/84/115*, and *250/250/283*.

Pseudohierarchical Decomposition

Although the clustering algorithm applied at each level is hierarchical, the stable features at each scale (or the number of clusters) are not necessarily hierarchical. In practice, there is still a great degree of overlap between clusters generated at different scales. Accordingly, it is possible to match clusters generated at different scales in a pseudohierarchical way, through inclusive masking. Specifically, we determined the overlap between each pair of clusters (across scales). Each cluster at scale N (higher scale, for example $N = 34$) was associated with the cluster at scale M (lower scale, for example $M = 4$), with which it had a maximal overlap (with $M < N$). Based on this correspondence, we were able to display the decomposition of each cluster from scale M to N.

Spatial and Temporal Consistencies of Task-evoked Networks

We implemented a series of statistical tests to assess the consistency of task-evoked networks across subjects both in the spatial domain (in terms of maps) and the temporal domain (in terms of FIR shape).

Spatial Consistency

We derived the average group stability between any region in the brain and all the regions in each of the group networks, resulting into a full brain stability map. To limit the influence of parts of the brain with loosely defined cluster assignment, the regions within each cluster were ordered by descending average stability, and the top 50% (called "stable cores") were retained. The stability maps were recomputed using only the stable cores for averaging. We observed that even in the absence of any task (i.e., resting-state data), BASC-FIR would identify stable task-evoked networks because of the spatial similarity of noise fluctuations (Supplementary Fig. 4). To ensure that nonsignificant FIR would not drive stable clusters, we added "judo" noise to the original dataset for each bootstrap sample, at the individual level. The judo noise was generated by shuffling the event times, using the same shuffling for all brain regions. The judo noise was called this way because the technique rests upon the idea of turning the opponent's strength (the structured noise) to one's own advantage. By construction, no FIR estimate would be significant in the judo noise, but the spatial structure of task-independent fluctuations would be preserved. In addition to randomly permuting event times, the judo noise was also randomly permuted in space, such that a clustering based on this noise alone would exhibit absolutely no stability across replications. We found that an amplification factor of 4 for the additive noise was strong enough to be in a regime where nonsignificant FIR would hardly be associated with stable clusters, while significant FIR would still exhibit a strong enough amplitude to drive stable clusters (Supplementary Fig. 4). Based on this experiment, all exploratory analyses were conducted with an amplification factor of the judo noise of 4 and a stability threshold of 0.5. We verified that the arbitrary choice of a threshold of 0.5 on stability did not markedly impact the conclusions reported in the Results section (Supplementary Fig. 5).

Temporal Consistency

Although regions within a network share some similarity in their associated FIR shapes at the individual level, there is no guarantee that the FIR shapes are consistent across subjects for a group network. We implemented bootstrap-based tests to assess the significance of network-level FIR estimates at the group level, as well as the significance of the differences in FIR estimation between networks at the group level. For each scale, the average FIR across all subjects was derived based on the stable core of each group cluster. A confidence interval on the average FIR as well as on the difference between 2 average FIR associated with different clusters was derived by bootstrapping the subjects (Efron and Tibshirani 1994), with 10 000 samples. The bootstrap probability that the average FIR (or the difference in average FIR between 2 clusters) was equal to zero was derived using a bilateral (symmetric) test. Multiple comparisons across all clusters and time points were corrected by a false-discovery rate procedure (Benjamini and Yekutieli 2001), with a significance level of $q < 0.05$. As expected, we observed empirically that the amount of judo noise did not have an impact on the FIR tests in the temporal domain, both in the task data and in a control "rest" experiment (Supplementary Fig. 6).

Results

Our first objective was to demonstrate using cluster analysis that the richness of task-evoked responses is patterned enough to be systematically characterized across participants and multiple scales. Because of the exploratory nature of these analyses, results are shown for stability thresholded maps to assess the spatial consistency of task-evoked networks at the group level. We also report group-level statistics for the temporal dynamics of all reported networks and for their pairwise comparisons. Of note, we will refer to specific clusters as cXsY, where c stands for cluster and s denotes the scale used, for example, *c1s4* refers to cluster 1 observed at scale 4 (see Table 1, for a list of representative brain areas composing each cluster/network).

Four Main Networks and Their Associated Task-Evoked Temporal Dynamics

To get an understanding of the broad variety of dynamics elicited by the task, we first examined networks detected at scale 4

Table 1
Multiscale partition of the brain into stable task-evoked networks

Scale	Root	Cluster	MNI coordinates of slices in figures			Nomenclature—networks or key regions
			z	*y*	*x*	
S4		C1	−6	−75	−22	Visual network (occipital regions)
		C2	−19	−55	2	Default mode network (e.g., medial prefontal cortex, posterior cingulate cortex and inferior parietal lobule)
		C3	51	1	30	Motor preparation network (e.g., premotor cortical and subcortical regions)
		C4	53	−59	31	Motor execution network (e.g., sensorimotor cortical and subcortical regions)
S9		C1	−6	−80	22	Secondary visual areas
		C3	0	−75	7	Primary visual areas
		C4	−19	−55	2	Inferior parietal lobule, posterior cingulate cortex, medial prefrontal cortex, medial temporal lobe, temporal pole, cerebellar lobule 9
		C5	−23	−65	11	Superior medial parietal lobule, cerebellar crus 1/2
		C6	53	1	−3	pSMA, rostral cingulate motor area, rostro-Pmd, basal ganglia
		C7	10	−20	48	Auditory cortex
		C8	53	−55	11	SMA, caudal cingulate motor area, caudo-Pmd, superior lateral parietal lobule, cerebellar lobule/vermis 6
		C9	53	−62	−26	Sensorimotor cortex, cerebellar lobules/vermis 5 and 8
S34	C1S4	C1	−5		5	v3
		C2	5			Medial bank of sensorimotor cortex
		C3	15			v4
		C8	25			v2
		C9				v1
		C21				Inferior temporal lobe, orbitofrontal cortex
		C24				Anterior cingulate cortex, insula
	C2S4	C5	−35		5	Parieto-temporal junction
		C6	−15			Parahippocampus, cerebellar lobule 9, inferior parietal cortex
		C7	0			Cerebellar crus 2
		C10	30			Temporal lobe
		C11				Posterior cingulate cortex, precuneus
		C12				Hippocampus, temporal pole
		C13				Anterior medial prefrontal cortex
		C14				Ventral medial prefrontal cortex, inferior parietal cortex
		C17				Dorsal medial prefrontal cortex
		C20				Superior temporal lobe
	C3S4	C15	28	−8	54	Ventral premotor cortex
		C16	45	41	−13	Superior medial parietal lobule
		C19	−27	−66	12	Medial cerebellar crus 1
		C23	21	20	−10	Frontopolar prefrontal cortex
		C27	2	5	27	Striatum, thalamus
		C28	−27	−65	−26	Lateral cerebellar crus 1
	C4S4	C30	53	0	5	(pre)SMA, cingulate motor area
		C31	13	−19	51	Auditory cortex
		C32	55	−53	−24	Superior lateral parietal lobule, cerebellar lobules/vermis 6 and 8
		C33	53	−11	−39	Left sensorimotor cortex
		C34	53	−55	51	Right sensorimotor cortex, cerebellar lobule/vermis 5

Note: Description of the results presented in Figures 1–3 (scales 4 and 9, as well as decompositions at scale 34 of the 4 clusters seen at scale 4). MNI coordinates (*z*, *y*, *x*) are given for slices represented in the Figures 1–3 following the same order. A basic network nomenclature or a list of the most notable brain regions is provided.

(Fig. 1). Two networks exhibited a negative (below baseline) response during movement execution (*c1s4* and *c2s4*). Network *c1s4* included primary and secondary visual regions in the occipital lobe. Network *c2s4* was an extended default mode network including the medial prefrontal cortex, posterior cingulate cortex, and bilateral inferior parietal cortex. The other 2 networks exhibited a positive response to both motor preparation and execution (*c3s4* and *c4s4*), as reflected by 2 successive bumps in the group average FIR. Both networks differed by their relative involvement in each task component: *c3s4* was composed of associative brain areas that responded more to the preparation phase, whereas *c4s4* included sensorimotor areas that responded more to the execution phase. These 2 task-positive networks encompassed both cortical and subcortical regions. Of note, the spatial distribution of stable networks at scale 4 closely matched a standard activation analysis performed using a fixed canonical hemodynamic response function (Supplementary Fig. 7).

Decomposition of the Task-Positive Networks Is Driven by a Gradient of Involvement in Motor Preparation Versus Execution

The decomposition from scale 4 to 9 was pseudohierarchical, that is, networks at scale 9 were approximately splits of the networks at scale 4 (Fig. 1 and Table 1; see also Supplementary Fig. 8 for surface-based representations). For example, the visual network was split into primary and secondary visual areas (*c1s9* and *c3s9*). At scale 9, many between-network differences in task-evoked temporal dynamics remained significant. As an example, the medial visual areas showed a positive inflection at execution onset, significantly higher than the activation level of lateral visual areas. Furthermore, networks *c5s9* and *c6s9* appeared as a split of the associative network *c3s4*, whereas networks *c8s9* and *c9s9* were a split of the sensorimotor network *c4s4*. Compared with networks *c5s9* and *c9s9*, networks *c6s9* and *c8s9* exhibited a much more balanced contribution between the preparation and execution phases,

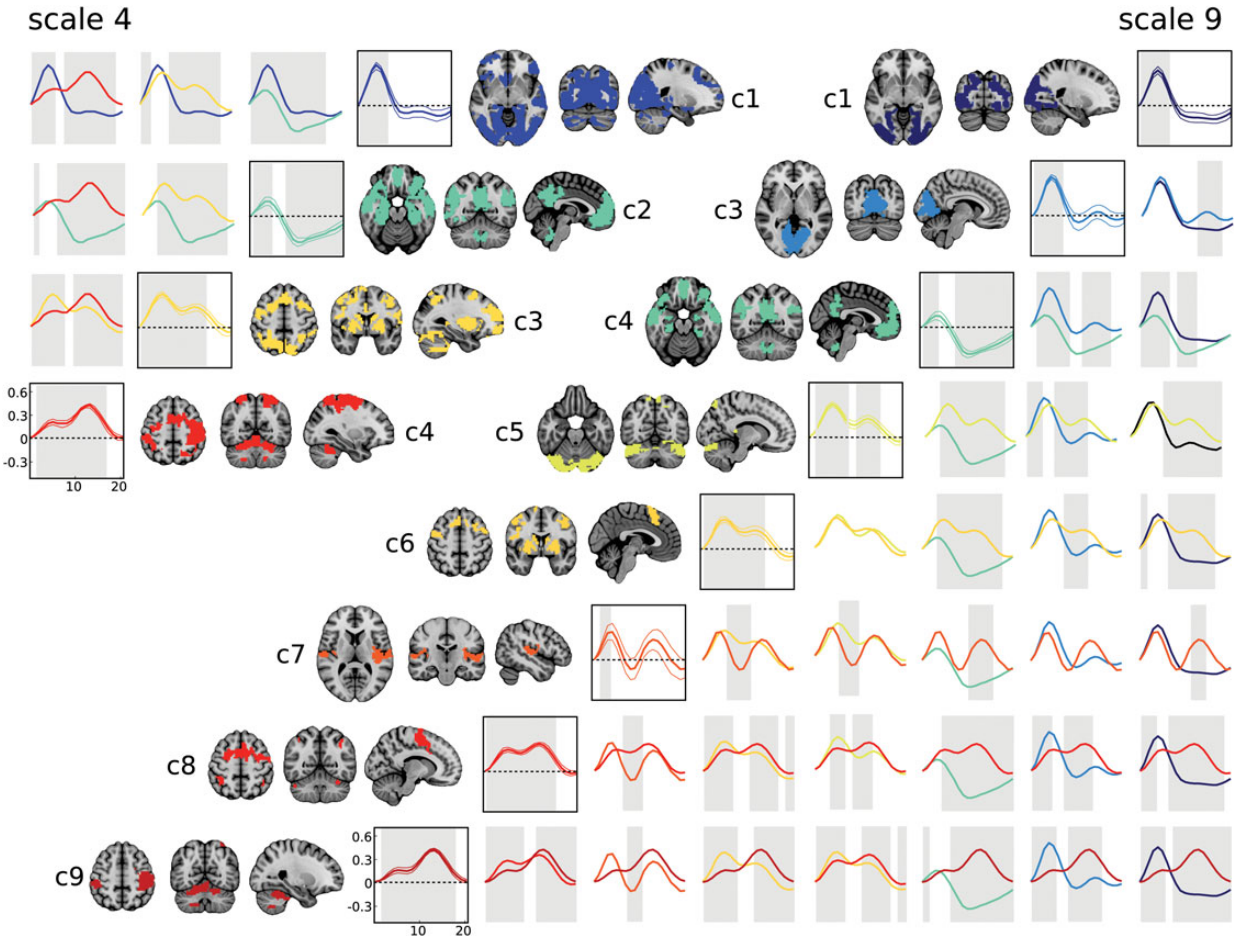

Figure 1. Group-level task-evoked networks. Group task-evoked networks at scales 4 and 9 (threshold based on a stability of >0.5). The order of networks is defined based on the difference value between the response peaks for the preparation and execution components of the task. Axial, coronal, and sagittal slices are superimposed onto the MNI nonlinear template. The mean estimated response profile for each network is given with its 95% confidence interval (color-matched shadowed area) on the adjacent diagonal. Time points of the task-evoked response that significantly differ from 0 are highlighted with a gray background ($q < 0.05$). Pairwise comparisons of the clusters' evoked responses are shown in off-diagonal squares, the gray background indicating in this case the significance of the difference at each time point ($q < 0.05$). Note that network *c2s9* is not included in this figure because no region survived a stability threshold of 0.5.

although each network still exhibited a marked preference (preparation for *c6s9* and execution for *c8s9*). Scale 9 thus revealed a gradient of involvement in the preparation versus execution phases of the task, reflected in separate task-evoked networks.

Higher Decomposition of Task-Positive Networks Is Associated with Subtle Differences in Task-Evoked Dynamics

Following the observation of a preparation versus execution gradient in larger-scale networks, we investigated how the preparation versus execution gradient further influenced the decomposition of the 2 main task-positive networks (*c3s4* and *c4s4*) into subnetworks at scale 34 (Fig. 2 and Table 1). Most clusters remained symmetrical, but were much less distributed compared with lower scale decompositions (4 and 9). Importantly, networks still exhibited significant differences in task-evoked group dynamics.

To highlight the complex gradient of task-evoked activations, we ordered the networks based on the difference in their peak responses during preparation versus execution. This representation clearly showed that the associative and sensorimotor networks seen at scale 4 (*c3s4* and *c4s4*) precisely matched the cutoff between networks that respond more to preparation than execution at scale 34 (Fig. 2). However, subtle differences in task-evoked temporal dynamics were not only related to the gradient of involvement in preparation versus execution. For instance, the gain of response amplitude for preparation was significantly faster in *c16s34* than in *c19s34*, although these 2 clusters had very similar differences in peak responses to preparation versus execution.

Spatially stable task-positive networks were thus associated with significant differences in task-evoked dynamics at scale 34, whether related to the difference of involvement in preparation versus execution or to subtle variations in temporal delays. This is worth emphasizing since our multivariate analysis was only designed to capture spatially consistent networks across subjects, regardless of the temporal consistency of task-evoked dynamics at the group level. In contrast to the task-positive network decompositions described above, both the visual cortex and default mode network were decomposed into spatially stable subnetworks at scale 34, but we observed fewer significant differences between the clusters' temporal dynamics

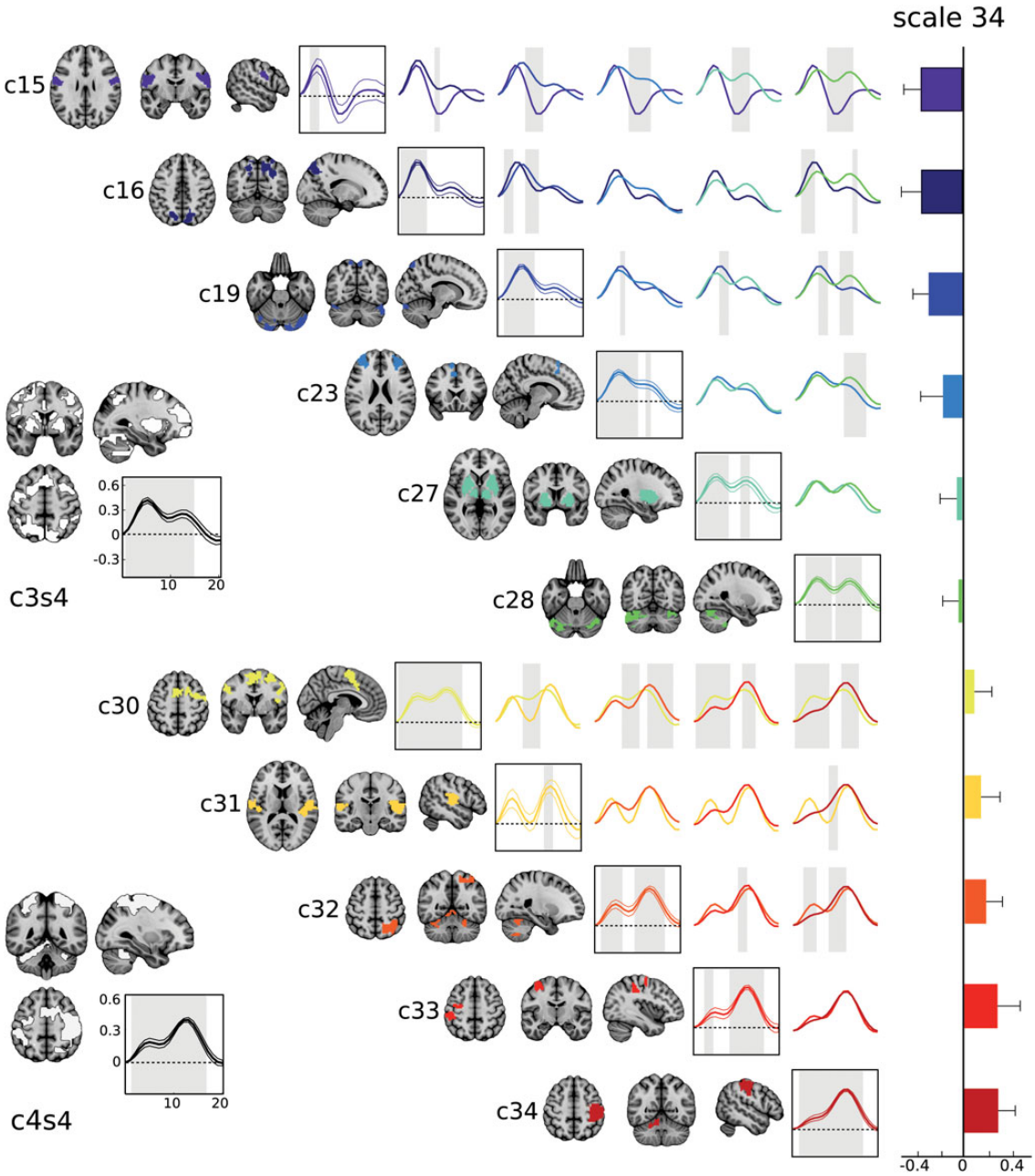

Figure 2. Decomposition of task-positive networks into subnetworks. The group-level networks (threshold based on a stability of >0.5) at scale 34 that overlapped with the 2 task-positive networks from scale 4 (c3s4, preparation > execution, and c4s4, execution > preparation) are presented. For reference, the networks c3s4 and c4s4 from scale 4 are shown as stroke white maps. Networks are shown with their response profiles (mean; confidence interval, color-matched shadowed area; test of significance against baseline at $q < 0.05$, gray background) as well as with pairwise comparisons between them (test of significance at $q < 0.05$). Axial, coronal, and sagittal slices are superimposed onto the MNI nonlinear template. The order of the networks is defined based on the difference in response peaks to the preparation and execution components of the task. This gradient is further highlighted in the right-side plot, where the magnitude of color-matched bars is determined by the subtraction of the peaks at execution minus preparation for each cluster (error bars show the 95% confidence interval on the mean).

at the group level (Fig. 3). Importantly, the decompositions still revealed plausible, stable clusters. First, the network that includes the occipital cortex at scale 4 (*c1s4*) was notably split at scale 34 into 4 symmetrical networks that correspond well with visual areas v1, v2, v3, and v4. Secondly, the extended default mode network observed at scale 4 (*c2s4*) was split into 10 networks at scale 34, covering for instance the medial prefrontal cortex (which was further divided into 3 parts along a ventro-dorsal axis), the hippocampus and parahippocampus, the temporal pole, the posterior cingulate cortex, the inferior parietal cortex, and lobule 9 of the cerebellum.

In the next sections, we proceeded with testing several predictions to assess the biological relevance of the observed task-evoked networks. Because these analyses were hypothesis-driven and we already established the stability of the observed group-level networks, we now report stability unthresholded (consensus) maps and do not further assess the significance of temporal dynamics within and between networks.

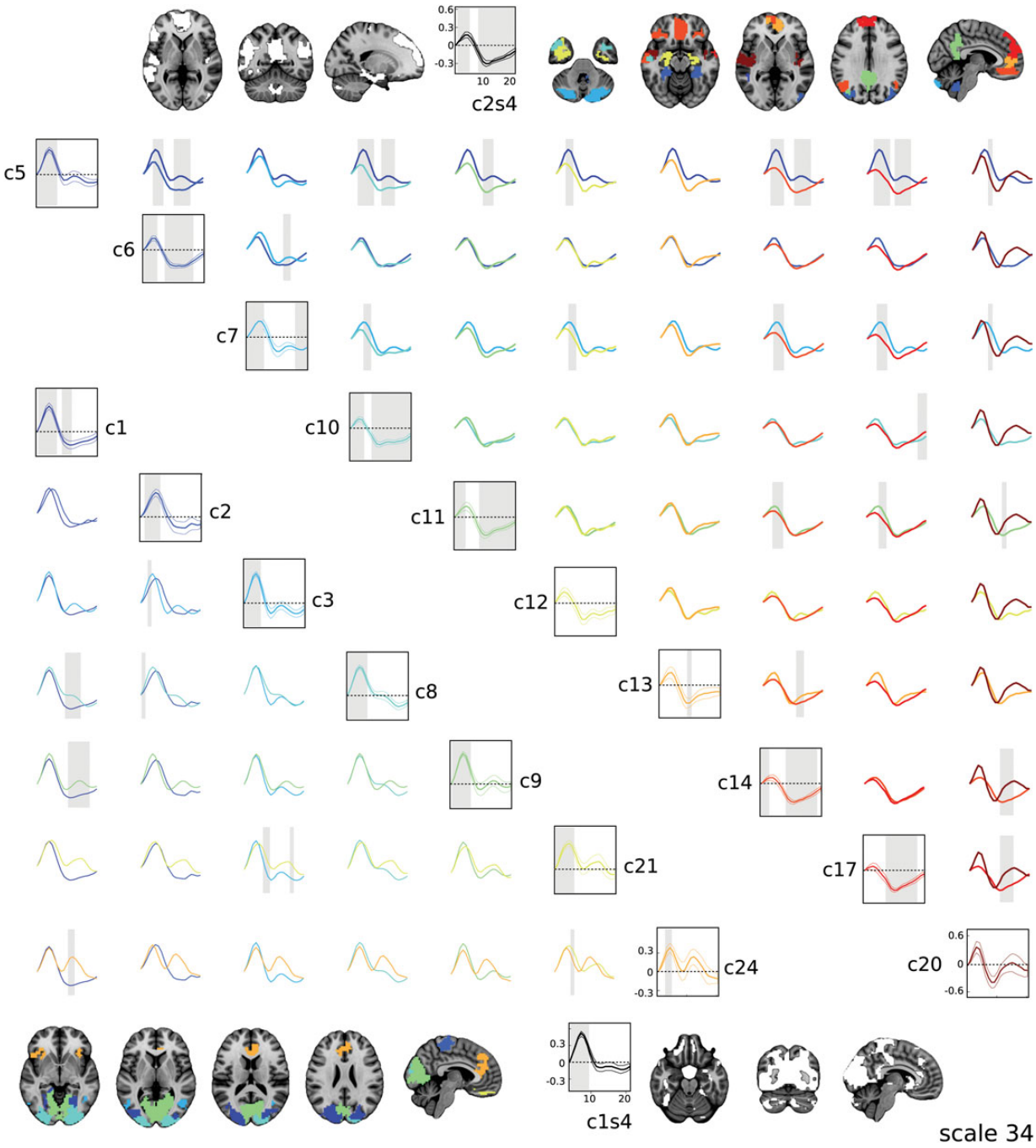

Figure 3. Decompositions of the visual and default mode networks into subnetworks. Group-level task-evoked networks (threshold based on a stability of >.5) at scale 34 that overlapped with the visual network (c1s4) and default mode network (c2s4) at scale 4 are presented in compound maps. The networks c1s4 and c2s4 from scale 4 are shown as stroke white maps for reference. Response profiles (mean; confidence interval, color-matched shadowed area; test of significance against baseline at $q < 0.05$, gray background) are shown for each cluster using the same color code, as well as with pairwise comparisons between them (test of significance at $q < 0.05$). Axial and sagittal slices are superimposed onto the MNI nonlinear template.

Rostro-caudal Functional Gradient in the Frontal Lobe

We first tested whether regions in the frontal cortex adhered to a gradient on an anterior–posterior axis, evolving from supporting higher-level cognitive processes serving motor preparation toward a tight coupling with motor execution. To test this hypothesis, we examined the 4 consensus networks that responded positively to the task at scale 9 (i.e., excluding the default mode network) and best overlapped with a series of anatomical areas of interest: Brodmann areas BA3 (postcentral gyrus), BA4/6/8 (superior frontal gyrus), BA9/46/10 (middle frontal gyrus), and BA24/32 (anterior cingulate gyrus) (i.e., excluding the visual networks). Each consensus network was color-coded based on the difference in the peak responses to execution minus preparation (Fig. 4). With only 2 instances that contradict our prediction, the overall pattern of results showed that the relative hemodynamic response to execution versus preparation overall increased when moving posteriorly from the prefrontal cortex to the hand region of the PMC.

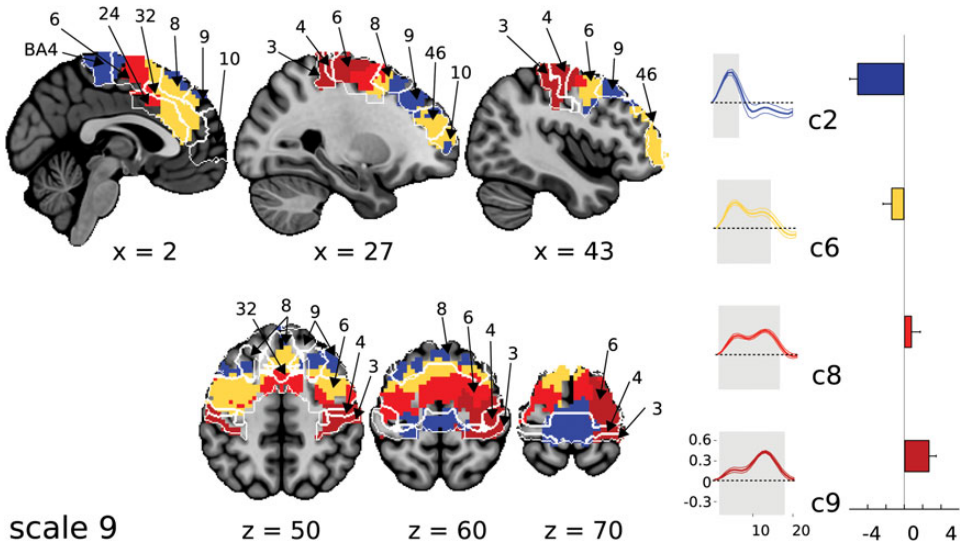

Figure 4. Rostro-caudal functional gradient in frontal areas. A composite consensus (stability unthresholded) map is shown at scale 9 for 4 clusters extending into the middle/superior frontal lobe. The functional gradient is highlighted in the bar plot, where the magnitude of color-matched bars is determined by the subtraction of the peaks at execution minus preparation for each cluster (error bars show the confidence interval on the mean). The response profiles (mean; confidence interval, color-matched shadowed area; test of significance against baseline at $q < 0.05$, gray background) are shown separately for each of the 4 clusters. Consensus maps are inclusively masked with a selected series of Brodmann areas (BA3, 4, 6, 8, 9, 10, 24, 32, and 46). The Brodmann areas template is part of mricron (http://www.nitrc.org/projects/mricron, last accessed on 24 March 2014). MNI coordinates are given for representative axial slices superimposed onto the MNI nonlinear template.

Specifically, network c2s9 showed higher activation during motor preparation than execution, with the response inflection at execution onset remaining below baseline activity. This network was located in the most anterior frontal areas (BA9 and BA8), but also posteriorly in the medial wall of BA4 contrary to our prediction. Network *c6s9* exhibited a higher response to preparation than execution, but significantly responded to execution too. It covered the most anterior portions of the pSMA (BA6), and of the ventral and dorsal cingulate motor areas (BA24 and BA32). Of note, it also extended laterally into the dorsolateral prefrontal cortex (BA46), anterior to network *c2s9* contrary to our hypothesis. Next, network c8s9 responded more to execution than preparation and was located posteriorly in Pmd and SMA proper (BA6). This network also extended into the caudal portion of the ventral and dorsal cingulate motor areas (BA24 and BA32). Finally, the network that showed the highest relative response to motor execution (*c9s9*) covered the most caudal (pre)motor cortex (BA6 and BA4) and somatosensory cortex (BA3). Note that the spatial extent of this motor execution network in the PMC was restricted to the hand area of the right hemisphere, contralateral to the (left) fingers used to perform the motor task.

Large-Scale Task-Evoked Cerebro-cerebellar Networks

We next examined the 6 task-evoked consensus networks that spread into both the cerebrum and cerebellum at scale 9 (Fig. 5). Our results indicated that the "motor" cerebellum was functionally connected to (pre)motor areas, while the "cognitive" cerebellum was functionally coupled with more cognitive regions such as the prefrontal and parietal cortical regions. The cerebellar lobule IX showed a task-evoked response similar to that of the default mode cerebral network (*c4s9*). Cerebellar crus II was part of a network that notably included the ventrolateral prefrontal cortex, the hippocampal complex, dorsal fronto-parietal areas, and the posterior cingulate cortex (*c2s9*). Crus I and lobule VIIb of the cerebellum were functionally connected to the ventromedial prefrontal cortex and medial superior parietal cortex (*c5s9*). In network c6s9, a limited lateral area of crus I was functionally coupled with the rostral portion of the premotor and anterior cingulate cortices as well as the basal ganglia. Subregions of the cerebellar lobule VI were essentially connected to the caudal regions of the premotor and anterior cingulate cortical regions (*c8s9*). Finally, the lobules V, VI, and VIII of the cerebellum were part of the network covering the sensorimotor cortex (*c9s9*). Of note, the only task-evoked networks that did not also include cerebellar territories at scale 9 were the primary visual and auditory cortices (*c1s9*, *c3s9*, and *c7s9*).

Fine-Grained Parcellation of the Basal Ganglia

Finally, we expected that the pseudohierarchy of task-evoked networks reflected the organization of cortico-basal ganglia loops, akin to the result obtained for task-evoked cortico-cerebellar loops. In contrast with the cerebellum, however, the basal ganglia was not split into distinct distributed clusters at any of the scales reported so far (i.e., scales 4, 9, and 34). Clusters in the basal ganglia turned out to be most stable at higher scales with local, rather than distributed, networks (Supplementary Fig. 5). Therefore, we explored scales 115 and 283 to determine whether distinct territories within the basal ganglia could nonetheless be unraveled.

Stable parcellations were similarly found at both scales and provided redundant findings. Here, we only report findings at scale 283. At this scale, several consensus networks isolated the putamen, caudate nucleus, and thalamus, each of these subcortical structures being further subdivided into 3 symmetrical parcels (Fig. 6). Symmetrical anterior and posterior territories of the putamen were dissociated from one another. Similarly, distinct bilateral subregions of the caudate nucleus were distinguished along the rostro-caudal axis. Most subregions in the basal ganglia showed a higher response to motor preparation than execution. However, this relative preference for motor preparation versus execution diminished from anterior to posterior subregions, akin to the functional gradient seen in the frontal lobe.

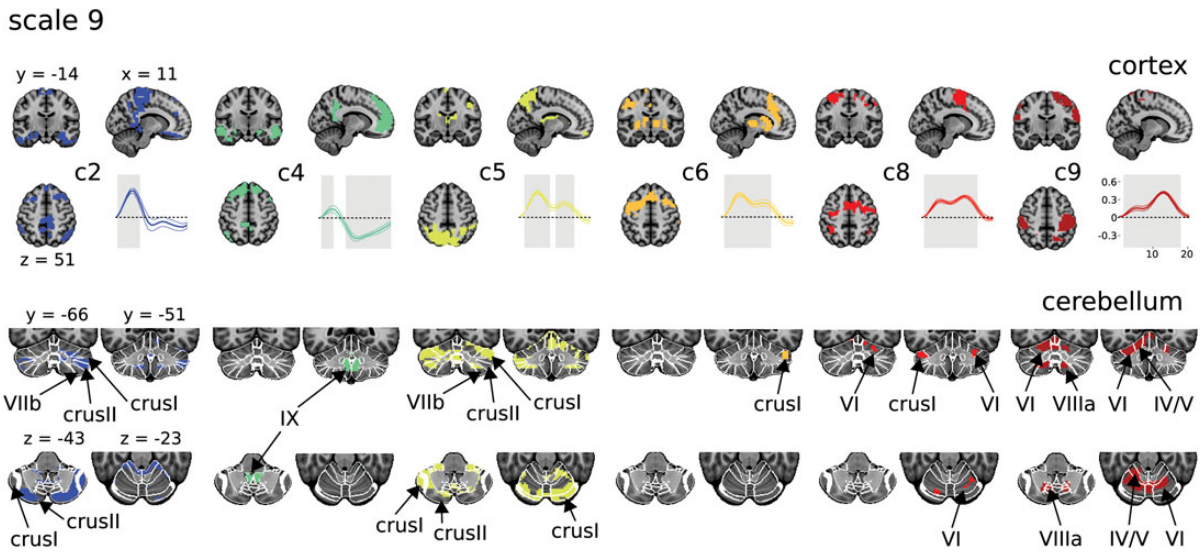

Figure 5. Distributed cerebro-cerebellar task-evoked networks. Six consensus (stability unthresholded) clusters that extend into both the cerebrum and cerebellum at scale 9 are shown along with their response profiles (mean; confidence interval, color-matched shadowed area; test of significance against baseline at $q < 0.05$, gray background). Maps are superimposed onto sections of the MNI nonlinear template. The same axial, coronal, and sagittal slices (MNI coordinates) are selected to display the 6 clusters, either in the cerebrum or cerebellum. White delineations of cerebellar territories are obtained from a probabilistic atlas of the cerebellum (Diedrichsen et al. 2009), with the legends highlighting those lobules that best overlap with the spatial map of each cluster.

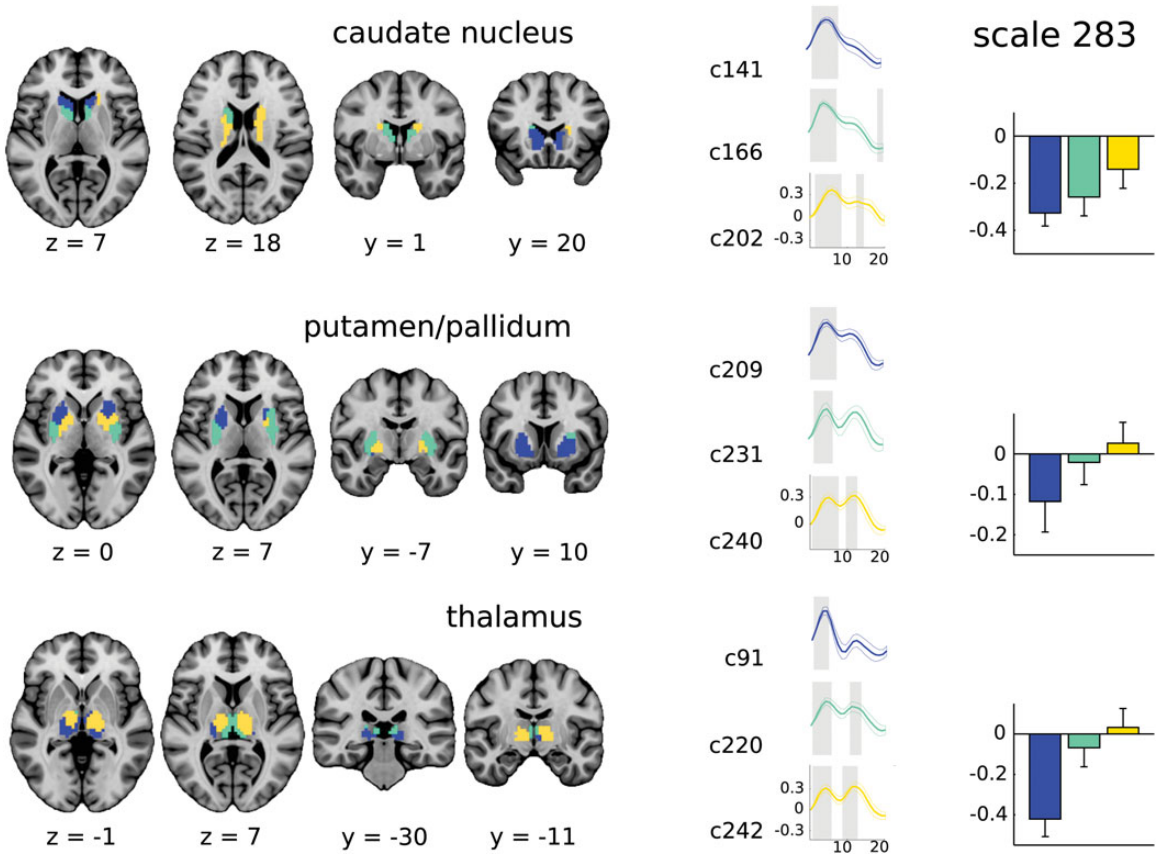

Figure 6. Discrete divisions of basal ganglia components. Three consensus (stability unthreshold) networks at scale 283 are shown along with their response profiles for each of 3 basal ganglia regions: the caudate nucleus, the putamen/pallidum complex, and the thalamus. Clusters are colored based on the relative involvement of each region's territories in the preparation versus execution components of the task. This gradient is reflected in the bar plots, where the magnitude of color-matched bars is determined by the subtraction of the peaks at execution minus preparation for each cluster (error bars show the 95% confidence interval on the mean). MNI coordinates are given for informative axial and coronal slices. Maps are superimposed onto the MNI nonlinear template.

Discussion

Uncovering the Spatio-temporal Organization of Task-Evoked Activity

Our findings show that the rich variety of hemodynamic responses elicited by a motor task is systematic enough to decompose the whole human brain into stable task-evoked networks at the group level. Recent work by Gonzalez-Castillo et al. (2012) demonstrated the existence of distinct task-evoked networks across the entire brain in individual subjects using massive averaging of extremely long time series. In their simple visual task, it was however difficult to evaluate whether those task-evoked networks reflected general principles of brain organization or simply idiosyncratic individual differences. Here, by leveraging the stability of networks across subjects, we derived group-level networks using a sample size typical in a task-based fMRI study (~20 subjects) and with a reasonable task duration per subject (~50 trials).

We derived a pseudohierarchy of task-evoked networks, in line with evidence suggesting that the brain adheres to a hierarchical organization (Smith et al. 2009; Meunier et al. 2010; Power et al. 2011; Yeo et al. 2011; Kelly et al. 2012). Two aspects of our multiscale decompositions strongly suggested that they were functionally meaningful. First, the network decomposition was largely driven by a gradient of involvement in motor preparation versus execution. This gradient evolved on a rostro-caudal axis for several areas in the frontal lobe. Secondly, the spatial network arrangement of various regions of the cortex and cerebellum was consistent with known cerebro-cerebellar fiber tracts. Likewise, task-evoked parcellations of the basal ganglia corresponded well to anatomical subterritories known to be connected with distinct cortical areas. The present work thus establishes that subtle differences in task-evoked dynamics reflect biologically meaningful mechanisms.

Insights Into the Brain Correlates of Motor Control

The spatial distribution of the 2 task-positive networks observed at scale 4 was consistent with binarized activation maps reported for delayed sequential motor tasks (Gerardin et al. 2004; Boecker et al. 2008; Jankowski et al. 2009; Supplementary Fig. 7). However, our task-evoked networks exhibited different temporal characteristics compared with classical activation maps. Typical activation maps reveal little overlap between brain areas activated by both motor preparation and execution. In contrast, the 2 task-positive networks observed at scale 4 exhibited significant responses to both task components, with a gradient of involvement in preparation versus execution.

The functional organization observed at scale 9, and above, supports the idea that this functional gradient evolved along a rostro-caudal axis in frontal regions. This was especially true for networks that were primarily involved in both components of the task, as they showed decreasing responses to preparation and increasing responses to execution when moving from prefrontal to sensorimotor cortex. However, in the case of the one network that did not show a significant response to motor execution, a contradictory pattern was observed for the area 9 of the dorsolateral prefrontal cortex and the medial bank of the sensorimotor cortex. Using a data-mining method as in the present work may thus reveal that not all areas of the frontal lobe follow a strict antero-posterior gradient. However, this conclusion must be taken with some caution because this network was characterized by a low stability and associated with a high variance of its task-evoked response at the group level. Hence, the observed organization of task-evoked activity is overall in line with predicted properties of the frontal lobe (Nachev et al. 2008; Badre and D'Esposito 2009), as supported by FIR analyses in selected regions (Richter et al. 1997; Wildgruber et al. 1997; Weilke et al. 2001). This result is also reminiscent of monkey electrophysiology studies, showing that numerous regions in the frontal lobe contain neurons that respond to both motor preparation and execution (Okano and Tanji 1987; Romo and Schultz 1987; Mushiake et al. 1991). Yet, the proportion of specific neurons varied smoothly from one region to another (Passingham et al. 2002).

Few fMRI studies on internally generated movements have characterized task-evoked dynamics outside the frontal lobe. Specific examinations focused on selected regions within the parietal lobe, the basal ganglia or cerebellum (Cui et al. 2000; Elsinger et al. 2006). The present results showed that stable task-evoked networks covered extensive cortical and subcortical territories. Our findings thus highlight the relevance of studying task-evoked activity in the entire brain, and suggest a large specificity in how a given cognitive context translates into the modulation of activity for numerous brain regions.

Neurophysiological Basis of Task-Evoked Networks

The distributed task-evoked networks observed at low scales were governed by large-scale connectivity. Our decompositions grouped the lobules IV, V, VI, and VIII of the cerebellum and (pre)motor areas. In contrast, crus I and II as well as lobules VII and IX of the cerebellum were associated with more cognitive regions, such as prefrontal and parietal cortical regions. These findings are in good agreement with known properties of cerebro-cerebellar circuits (Middleton and Strick 2000; Bostan et al. 2013) shown in humans with resting-state fMRI (O'Reilly et al. 2010; Buckner et al. 2011) and diffusion-weighted imaging (Salmi et al. 2010), or virus transneuronal tracers in nonhuman primates (Hoover and Strick 1999; Kelly and Strick 2003; Akkal et al. 2007). Of note, only the primary visual and auditory networks (*c1s9*, *c3s9*, and *c7s9*) did not include cerebellar territories at scale 9. This result fits well with previous evidence for an absence of cerebellar representation for those 2 cortical networks (Buckner et al. 2011).

In the basal ganglia, we did not observe different subterritories associated with distinct cortical areas at low scales. This is likely due to the fact that task-evoked responses in the basal ganglia were dominated by motor preparation, in contrast with the large variety of responses seen in the cortex and cerebellum. A secondary cause might be the impact of local smoothness in a set of spatially isolated areas, a factor that has less impact in cortical and cerebellar territories. Yet, the structures of the basal ganglia (putamen, caudate nucleus, and thalamus) did each decompose into several bilateral task-evoked parcels at high scales. The obtained parcels matched well with subterritories of the basal ganglia associated with different functions, for instance supporting associative versus sensorimotor processes (Alexander and Crutcher 1990; Middleton and Strick 2000). In the literature, similar subterritories were defined by cortico-subcortical pathways, as shown in humans by resting-state fMRI (Zhang et al. 2010; Choi et al. 2012) and diffusion-weighted

imaging (Draganski et al. 2008), or neuroanatomical research in monkeys (Hoover and Strick 1999; Akkal et al. 2007).

A Network Approach to Task-Based fMRI

Recent research clearly supports the notion that extrinsic, task-evoked networks exhibit many similarities with intrinsic, resting-state networks. Connectivity methods applied to large meta-analyses of task-based fMRI data have described networks that can be related to many general cognitive domains while exhibiting good correspondence to commonly observed resting-state networks (Toro et al. 2008; Smith et al. 2009; Laird et al. 2013). Accordingly, it is worth noting that the task-evoked default mode and visual subnetworks observed here match with parcellations derived using resting-state fMRI (Andrews-Hanna et al. 2010; Wilms et al. 2010).

Although extrinsic and intrinsic functional brain architectures exhibit great similarity, they are not equivalent (Mennes et al. 2013), and it is clear that task performance does modulate functional interactions in the brain (Mennes et al. 2011; Gordon et al. 2012). The use of a motor task in the current study translated into a highly asymmetric sensorimotor task-evoked network, while the sensorimotor network derived from resting-state fMRI is generally symmetrical (Bellec et al. 2010; Power et al. 2011; Yeo et al. 2011). Similarly, while resting-state fMRI studies typically do not reveal a subdivision of the intrinsic motor network, the task-evoked networks obtained here reveal several (pre)motor subnetworks even at low scales with 4 or 9 networks. Hence, studying the richness of task-evoked networks provides a unique window into the brain in action, with the advantage that specific inferences can be drawn regarding the roles of particular networks in specific cognitive contexts.

Task-based fMRI is often viewed as a characterization of brain segregation, with a limited number of brain regions selectively engaged in a cognitive process. In contrast, resting-state fMRI has become increasingly popular to map functional integration processes and to describe fundamental properties of brain organization. Our work shows that mining task-evoked responses derived from a single task-based fMRI experiment can capture the multiscale network organization of the brain. A notable advantage of task-evoked networks is that they are interpretable with respect to the mental processes and specific modulations associated with the experimental paradigm. In addition, our approach is attractive to characterize the effect of a given task in a group of individuals, but also allows investigating differences in task-evoked responses between different tasks or populations. The ability to accurately characterize task-evoked dynamics through the exploration of extrinsic network hierarchies could therefore provide new insights into the neural basis of cognition.

Supplementary Material

Supplementary material can be found at: http://www.cercor.oxfordjournals.org/.

Funding

This work was supported by grants from the Natural Sciences and Engineering Research Council of Canada (NSERC #42909-209) and the Canadian Institutes of Health Research (CIHR #MOP-97830) to J.D., as well as a grant from the Natural Sciences and Engineering Research Council of Canada (NSERC #436141) to P.B. P.O. is supported by a postdoctoral research fellowship from the Canadian Institutes of Health Research (CIHR), and P.B. is supported by a salary award of the Fonds de Recherche du Québec—Santé (FRQS).

Notes

Conflict of Interest: None declared.

References

Akkal D, Dum RP, Strick PL. 2007. Supplementary motor area and presupplementary motor area: targets of basal ganglia and cerebellar ouput. J Neurosci. 27:10659–10673.

Alexander GE, Crutcher MD. 1990. Functional architecture of basal ganglia circuits: neural substrates of parallel processing. Trends Neurosci. 13:266–271.

Andrews-Hanna JR, Reidler JS, Sepulcre J, Poulin R, Buckner RL. 2010. Functional-anatomic fractionation of the brain's default network. Neuron. 65:550–562.

Badre D, D'Esposito M. 2009. Is the rostro-caudal axis of the frontal lobe hierarchical? Nat Rev Neurosci. 10:659–669.

Bellec P. 2013. Mining the hierarchy of resting-state brain networks: selection of representative clusters in a multiscale structure. Proceedings of the 2013 International Workshop on Pattern Recognition in Neuroimaging, IEEE, p. 54–57.

Bellec P, Lavoie-Courchesne S, Dickinson P, Lerch JP, Zijdenbos AP, Evans AC. 2012. The pipeline system for Octave and Matlab (PSOM): a lightweight scripting framework and execution engine for scientific workflows. Front Neuroinform. 6:7.

Bellec P, Perlbarg V, Jbabdi S, Pélégrini-Issac M, Anton J-L, Doyon J, Benali H. 2006. Identification of large-scale networks in the brain using fMRI. Neuroimage. 29:1231–1243.

Bellec P, Rosa-Neto P, Lyttelton OC, Benali H, Evans AC. 2010. Multilevel bootstrap analysis of stable clusters in resting-state fMRI. Neuroimage. 51:1126–1139.

Benjamini Y, Yekutieli D. 2001. The control of the false discovery rate in multiple testing under dependency. Ann Stat. 29:1165–1188.

Boecker H, Jankowski J, Ditter P, Scheef L. 2008. A role of the basal ganglia and midbrain nuclei for initiation of motor sequences. Neuroimage. 39:1356–1369.

Bostan AC, Dum RP, Strick PL. 2013. Cerebellar networks with the cerebral cortex and basal ganglia. Trends Cogn Sci. 17:241–254.

Buckner RL, Krienen FM, Castellanos A, Diaz JC, Yeo BTT. 2011. The organization of the human cerebellum estimated by intrinsic functional connectivity. J Neurophysiol. 106:2322–2345.

Calhoun VD, Adali T, Pearlson GD, Pekar JJ. 2001. A method for making group inferences from functional MRI data using independent component analysis. Hum Brain Mapp. 14:140–151.

Choi EY, Yeo BTT, Buckner RL. 2012. The organization of the human striatum estimated by intrinsic functional connectivity. J Neurophysiol. 108:2242–2263.

Collins DL, Neelin P, Peters TM, Evans AC. 1994. Automatic 3D intersubject registration of MR volumetric data in standardized Talairach space. J Comput Assist Tomogr. 18:192–205.

Cui SZ, Li EZ, Zang YF, Weng XC, Ivry R, Wang JJ. 2000. Both sides of human cerebellum involved in preparation and execution of sequential movements. Neuroreport. 11:3849–3853.

Dale AM, Buckner RL. 1997. Selective averaging of rapidly presented individual trials using fMRI. Hum Brain Mapp. 5:329–340.

d'Avossa G, Shulman GL, Corbetta M. 2003. Identification of cerebral networks by classification of the shape of BOLD responses. J Neurophysiol. 90:360–371.

Diedrichsen J, Balsters JH, Flavell J, Cussans E, Ramnani N. 2009. A probabilistic MR Atlas of the human cerebellum. Neuroimage. 46:39–46.

Draganski B, Kherif F, Klöppel S, Cook PA, Alexander DC, Parker GJM, Deichmann R, Ashburner J, Frackowiak RSJ. 2008. Evidence for segregated and integrative connectivity patterns in the human basal ganglia. J Neurosci. 28:7143–7152.
Efron B, Tibshirani R. 1994. An Introduction to the Bootstrap. Boca Raton, Florida: Chapman and Hall/CRC.
Elsinger CL, Harrington DL, Rao SM. 2006. From preparation to online control: reappraisal of neural circuitry mediating internally generated and externally guided actions. Neuroimage. 31:1177–1187.
Gerardin E, Pochon J-B, Poline J-B, Tremblay L, Van de Moortele P-F, Levy R, Dubois B, Le Bihan D, Lehéricy S. 2004. Distinct striatal regions support movement selection, preparation and execution. Neuroreport. 15:2327–2331.
Gonzalez-Castillo J, Saad ZS, Handwerker DA, Inati SJ, Brenowitz N, Bandettini PA. 2012. Whole-brain, time-locked activation with simple tasks revealed using massive averaging and model-free analysis. Proc Natl Acad Sci USA. 109:5487–5492.
Gordon EM, Stollstorff M, Vaidya CJ. 2012. Using spatial multiple regression to identify intrinsic connectivity networks involved in working memory performance. Hum Brain Mapp. 33:1536–1552.
Hoover JE, Strick PL. 1999. The organization of cerebellar and basal ganglia outputs to primary motor cortex as revealed by retrograde transneuronal transport of herpes simplex virus type 1. J Neurosci. 19:1446–1463.
Jankowski J, Scheef L, Hüppe C, Boecker H. 2009. Distinct striatal regions for planning and executing novel and automated movement sequences. Neuroimage. 44:1369–1379.
Kelly C, Toro R, Di Martino A, Cox CL, Bellec P, Castellanos FX, Milham MP. 2012. A convergent functional architecture of the insula emerges across imaging modalities. Neuroimage. 61:1129–1142.
Kelly RM, Strick PL. 2003. Cerebellar loops with motor cortex and prefrontal cortex of nonhuman primates. J Neurosci. 23: 8432–8444.
Laird AR, Eickhoff SB, Rottschy C, Bzdok D, Ray KL, Fox PT. 2013. Networks of task co-activations. Neuroimage. 80:505–514.
Mennes M, Kelly C, Colcombe S, Castellanos FX, Milham MP. 2013. The extrinsic and intrinsic functional architectures of the human brain are not equivalent. Cereb Cortex. 23:223–229.
Mennes M, Zuo X-N, Kelly C, Di Martino A, Zang Y-F, Biswal B, Castellanos FX, Milham MP. 2011. Linking inter-individual differences in neural activation and behavior to intrinsic brain dynamics. Neuroimage. 54:2950–2959.
Metzak P, Feredoes E, Takane Y, Wang L, Weinstein S, Cairo T, Ngan ETC, Woodward TS. 2011. Constrained principal component analysis reveals functionally connected load-dependent networks involved in multiple stages of working memory. Hum Brain Mapp. 32:856–871.
Meunier D, Lambiotte R, Bullmore ET. 2010. Modular and hierarchically modular organization of brain networks. Front Neurosci. 4:200.
Middleton FA, Strick PL. 2000. Basal ganglia and cerebellar loops: motor and cognitive circuits. Brain Res Brain Res Rev. 31: 236–250.
Mushiake H, Inase M, Tanji J. 1991. Neuronal activity in the primate premotor, supplementary, and precentral motor cortex during visually guided and internally determined sequential movements. J Neurophysiol. 66:705–718.
Nachev P, Kennard C, Husain M. 2008. Functional role of the supplementary and pre-supplementary motor areas. Nat Rev Neurosci. 9:856–869.
Okano K, Tanji J. 1987. Neuronal activities in the primate motor fields of the agranular frontal cortex preceding visually triggered and self-paced movement. Exp Brain Res. 66:155–166.
O'Reilly JX, Beckmann CF, Tomassini V, Ramnani N, Johansen-Berg H. 2010. Distinct and overlapping functional zones in the cerebellum defined by resting state functional connectivity. Cereb Cortex. 20:953–965.
Passingham RE, Stephan KE, Kötter R. 2002. The anatomical basis of functional localization in the cortex. Nat Rev Neurosci. 3:606–616.
Power JD, Cohen AL, Nelson SM, Wig GS, Barnes KA, Church JA, Vogel AC, Laumann TO, Miezin FM, Schlaggar BL et al. 2011. Functional network organization of the human brain. Neuron. 72:665–678.
Richter W, Andersen PM, Georgopoulos AP, Kim SG. 1997. Sequential activity in human motor areas during a delayed cued finger movement task studied by time-resolved fMRI. Neuroreport. 8:1257–1261.
Romo R, Schultz W. 1987. Neuronal activity preceding self-initiated or externally timed arm movements in area 6 of monkey cortex. Exp Brain Res. 67:656–662.
Salmi J, Pallesen KJ, Neuvonen T, Brattico E, Korvenoja A, Salonen O, Carlson S. 2010. Cognitive and motor loops of the human cerebro-cerebellar system. J Cogn Neurosci. 22:2663–2676.
Smith SM, Fox PT, Miller KL, Glahn DC, Fox PM, Mackay CE, Filippini N, Watkins KE, Toro R, Laird AR et al. 2009. Correspondence of the brain's functional architecture during activation and rest. Proc Natl Acad Sci USA. 106:13040–13045.
Smolders A, De Martino F, Staeren N, Scheunders P, Sijbers J, Goebel R, Formisano E. 2007. Dissecting cognitive stages with time-resolved fMRI data: a comparison of fuzzy clustering and independent component analysis. Magn Reson Imaging. 25:860–868.
Svensén M, Kruggel F, Benali H. 2002. ICA of fMRI group study data. Neuroimage. 16:551–563.
Toro R, Fox PT, Paus T. 2008. Functional coactivation map of the human brain. Cereb Cortex. 18:2553–2559.
Weilke F, Spiegel S, Boecker H, von Einsiedel HG, Conrad B, Schwaiger M, Erhard P. 2001. Time-resolved fMRI of activation patterns in M1 and SMA during complex voluntary movement. J Neurophysiol. 85:1858–1863.
Wildgruber D, Erb M, Klose U, Grodd W. 1997. Sequential activation of supplementary motor area and primary motor cortex during self-paced finger movement in human evaluated by functional MRI. Neurosci Lett. 227:161–164.
Wilms M, Eickhoff SB, Hömke L, Rottschy C, Kujovic M, Amunts K, Fink GR. 2010. Comparison of functional and cytoarchitectonic maps of human visual areas V1, V2, V3d, V3v, and V4(v). Neuroimage. 49:1171–1179.
Worsley KJ. 2004. Developments in random field theory. In: Frackowiak R, editor-in-chief. Human brain function, 2nd ed. San Diego, California: Academic Press, p. 881–886.
Yeo BTT, Krienen FM, Sepulcre J, Sabuncu MR, Lashkari D, Hollinshead M, Roffman JL, Smoller JW, Zöllei L, Polimeni JR et al. 2011. The organization of the human cerebral cortex estimated by intrinsic functional connectivity. J Neurophysiol. 106:1125–1165.
Zhang D, Snyder AZ, Shimony JS, Fox MD, Raichle ME. 2010. Noninvasive functional and structural connectivity mapping of the human thalamocortical system. Cereb Cortex. 20:1187–1194.
Zijdenbos AP, Forghani R, Evans AC. 2002. Automatic "pipeline" analysis of 3-D MRI data for clinical trials: application to multiple sclerosis. IEEE Trans Med Imaging. 21:1280–1291.